Optics & Laser Technology 42 (2010) 1286–1293

Contents lists available at ScienceDirect

Optics & Laser Technology

journal homepage: www.elsevier.com/locate/optlastec

Broadband dispersion characteristics of diffractive microlenses based on the finite-difference time-domain method

Yuling Liu [a,*], Hua Liu [b], Liangfang He [a], Hanqing Zhou [a], Chenghua Sui [a]

[a] College of Science, Zhejiang University of Technology, Hangzhou 310014, China
[b] Opto_electronics technology center, Changchun Institute of Optics and Fine Mechanics and Physics, Chinese, Academy of Sciences, Changchun 130022, China

ARTICLE INFO

Article history:
Received 27 November 2009
Received in revised form
4 April 2010
Accepted 7 April 2010
Available online 24 April 2010

Keywords:
Diffractive microlens
Broadband Dispersion
Fiber Coupling

ABSTRACT

The broadband dispersion characteristics of diffractive microlenses are studied using the finite-difference time-domain (FDTD) method. The distributions of the diffracted electric fields obtained through a diffractive microlens are presented for illumination wavelengths ranging from 0.35 to 1.30 μm, along with the corresponding broadband dispersion curves. It is shown that both the principal focal length and the diffracted order of the principal focal point are dependent on the illumination wavelengths. The broadband dispersion characteristics of a diffractive microlens may be used to optimise light coupling for a broadband optical fibre source.

1. Introduction

Compared to refractive lenses, diffractive microlenses (DML) are more suitable for fibre coupling due to their micro-size and planar contour. Fabrication of a DML on a fibre tip for fibre-waveguide coupling was presented by Prasciolu et al. in 2003 [1]. Traditionally, a DML is normally designed for a monochromatic incident light. In recent years, however, researchers have presented broadband fibre sources [2,3] with exciting applications in diverse fields such as spectroscopy [4], optical coherence tomography [5], and high power wavelength-division multiplexing (WDM) [6]. For applications with broadband fibre sources, it is necessary to couple light of different incident wavelengths to a common spatial position. In this paper, we investigate the broadband dispersion characteristics of DMLs, demonstrate the relationship between incident wavelength and principal focal length, and present a potential solution to couple DMLs to a broadband fibre source.

Fig. 1 illustrates the case that normal incident plane waves are diffracted and focused on an optical axis via the DML zones. Several focal points appear on the optical axis. Different focal points are associated with different diffraction orders. The unfocused waves correspond to the zeroth diffraction order. Larger diffraction angles correspond to higher diffractive orders. The focal plane of the higher diffractive orders would be nearer to the surface of DML. However, focal points from different diffractive orders have dissimilar diffraction efficiencies. The energy distribution of the various diffraction orders is of great significance for high-throughput applications such as broadband fibre source coupling. Although the energy distribution has traditionally been analysed similarly to that of multiorder diffractive lenses [7,8], to our knowledge the broadband dispersion characteristics of DMLs have not been reported. For DML with a sub-wavelength minimum feature size, conventional scalar methods are not sufficiently accurate, and rigorous solutions of Maxwell's equations have to be solved to characterise such a structure.

In this paper, the broadband dispersion characteristics of DMLs are studied using the finite-difference time-domain (FDTD) method [9,10]. The design method of DML is given in Section 2, the FDTD method is detailed in Section 3, the simulation results and a broadband dispersion curve are presented in Section 4, and the implications and potential for broadband fibre coupling is described in Section 5.

2. Diffractive microlens design

In this work, the configuration of DML is designed to address applications with normal incident light with only on-axis focusing. For constructive interference at focal points, the zone radii are determined by the following expression:

$$\sqrt{r_k^2+f_{m,\lambda}^2}-f_{m,\lambda}=mk\lambda \tag{1}$$

as shown in Fig. 1, where r_k is the radius of kth zone, k ($k=1, 2, 3\ldots$) is the zone number, $f_{m,\lambda}$ is the mth-order focal length for the incident wavelength λ, and m ($m=0, \pm1, \pm2, \pm3\ldots$) is the

* Corresponding author.
E-mail address: lucy1971lyl@yahoo.com.cn (Y. Liu).

0030-3992/$ - see front matter © 2010 Elsevier Ltd. All rights reserved.
doi:10.1016/j.optlastec.2010.04.004

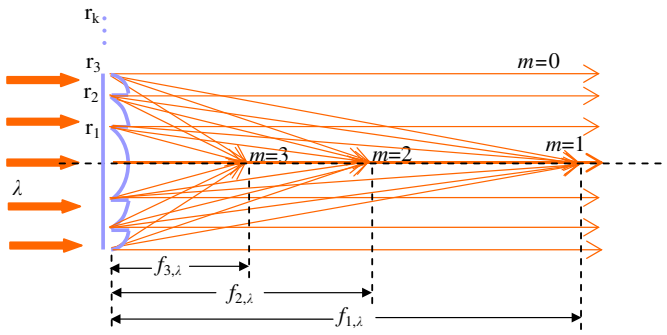

Fig. 1. Normal incident plane waves are diffracted and converged onto several focal points. The higher order foci correspond to shorter focal lengths.

diffractive order (the positive values of m lead to real foci, and negative values lead to virtual foci). The optical path length difference induced by adjacent zone boundaries is equal to $m\lambda$ for the diffraction order m. Focal length, $f_{m,\lambda}$, can be derived from Eq. (1) as follows:

$$f_{m,\lambda} = \frac{r_k^2}{2mk\lambda} - \frac{mk\lambda}{2} \tag{2}$$

A phase quantified technique is normally used to convert the continuous profile of a DML into a multilevel profile to ease the fabrication process. The radii of levels for a specific zone can be determined by the following expression:

$$r_{k,l} = \sqrt{2\lambda f[(k-1)+l/L]+\lambda^2[(k-1)+l/L]^2} \quad 1 \le l \le L \tag{3}$$

where $r_{k,l}$ is the zone radius of the lth level for a multilevel DML, and L is the total number of levels. The minimum feature size is achieved at the outermost step and is usually of sub-wavelength size. The etching depth of levels is determined by

$$h_l = \left(\frac{n_1\lambda}{n_2-n_1}\right)(L-l)/L \tag{4}$$

where n_1 and n_2 are refractive indices for air and DML material, respectively.

3. FDTD method

Light propagation through the DML is simulated using a FDTD method based on a rigorous vector solution of Maxwell's equations. A cylindrical DML is typically analysed using a two-dimensional FDTD method, whereas, for a circular DML, the body of revolution finite-difference time-domain (BOR FDTD) method is appropriate. Because the DML used in this paper is circular and axially symmetric, the BOR FDTD is used for analysis. The simulation space extends from the incident side of the DML to the transmitted far field (i.e., focusing field). The total-field/scatter-field technique is used to introduce the incident plane waves that excite the lattice. The DML structure is embedded in the lower part of the total field. On the boundary of the scatter-field, the perfectly matched layer (PML) absorbing boundary conditions (ABCs) are used to absorb outgoing waves. In this paper the parameter for the BOR FDTD are as follows: cell increments Δr and Δz are $\lambda/20$ (λ is the illumination wavelength), the time increment Δt is $\Delta z/2c$ (c is the speed of light in vacuum), and the PML thickness is 8 cells. The light source is a continuous sine wave that can be represented by $E=E_0\sin(2\pi fn\Delta t)$, where f is the illumination light frequency, and n is the time step number. The details of our simulation model can be found in Liu et al. [10].

4. FDTD simulation results and dispersion curve for broadband illumination light

The design parameters of the multilevel DML are as follows: the design wavelength is 1 μm, the design focal length is 25 μm, the refractive index of the material is 1.5, and the bottom thickness is 0.5 μm. There are 5 zones with 8 levels in each zone. The radius of the circular DML is 16.58 μm. The minimum feature size corresponding to the width of the outermost level is 0.23 μm, and the maximum etching depth is 1.75 μm. In the simulations, wavelengths ranging from 0.35 to 1.30 μm are used as the normally incident monochromatic light. The quantity we chose to monitor is the numerical value of the electric field amplitude $|E|$, where $|E|$ denotes the amplitude of the resultant electric field vector components E_r, E_ϕ, and E_z, and the field components are the direct results of BOR FDTD. Among several focal points on the optical axis, the focal point with maximal $|E|$ value is treated as the principal focus. Then the principal focal lengths (the distance along the optical axis between the innermost step of the multilevel DML and the principal focus) corresponding to these wavelengths are obtained. The focal depth is determined by the distance along the optical axis where $|E|$ is greater than 80% of the maximal $|E|$. The dispersion curve of the DML is plotted in subsection 4.4, where the relationship between principal focal lengths and incident wavelengths is illustrated.

4.1. Simulation results for illumination wavelengths of 1 μm

Fig. 2(a) shows that normal incident waves are diffracted and focused by the DML, the profile of the analysed DML is illustrated with a solid line, and the bright area represents the higher electric field amplitude. The $|E|$ along the optical axis is plotted in Fig. 2(b). The maximal value of $|E|$ on the optical axis determines the position of the principal focus. The principal focal length is 25.3 μm with 1-μm illumination, which is slightly longer than the designed focal length of 25 μm. The focal depth is 4.2 μm.

4.2. Simulation results for illumination wavelengths that are longer than 1 μm

The illumination wavelengths are as follows: 1.05, 1.10, 1.15, 1.20, 1.25, and 1.30 μm. The diffracted fields behind the DML are shown in Fig. 3(a)–(f). The maximum value of $|E|$ changes with illumination wavelengths. To show the focus position more clearly, the $|E|$ along the optical axis is normalised using the maximum value of $|E|$ and plotted in Fig. 4, from which the position of principal focus is determined. The principal focal lengths are 19.10, 19.80, 21.00, 21.65, 22.95, and 23.75 μm for illumination wavelengths of 1.30, 1.25, 1.20, 1.15, 1.10, and1.05 μm, respectively. The principal focal length increases with decreasing illumination wavelength for wavelengths between 1.0 and 1.30 μm. Compared with the focal lengths calculated according to Eq. (2), the principal foci obtained for the above wavelengths are of the 1st-order focus. The focal depths are 3.3, 3.4, 3.5, 3.6, 3.8, and 4.0 μm at illumination wavelengths of 1.30, 1.25, 1.20, 1.15, 1.10, and 1.05 μm, respectively. Therefore, the focal depth for the 1st-order focuses increases as the illumination wavelength decreases.

4.3. Simulation results for illumination wavelengths that are shorter than 1 μm

For simplicity, the simulation results are divided into two groups. The illumination wavelengths for the first group are 0.95, 0.90, 0.85 and 0.80 μm. The corresponding numerical results from

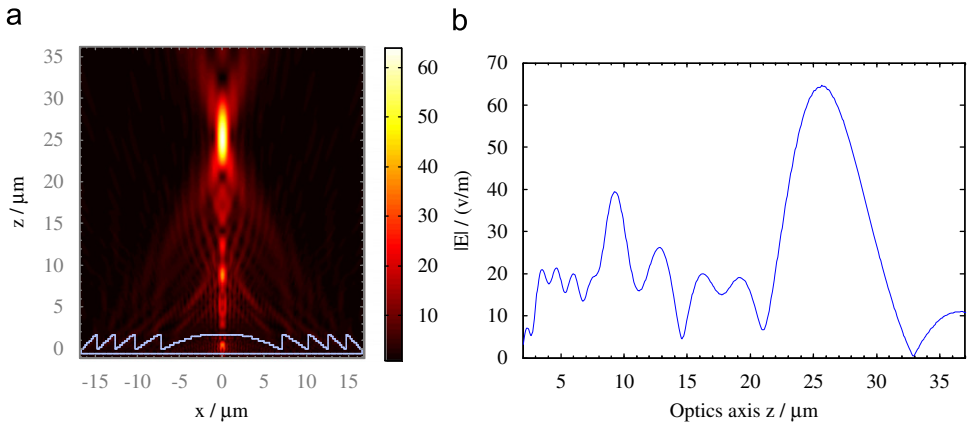

Fig. 2. Simulation results for the multilevel DML. (a) $|E|$ fields show a diffractive field distribution, (b) $|E|$ along the optical axis z (x=0) for an illumination wavelength of 1 μm.

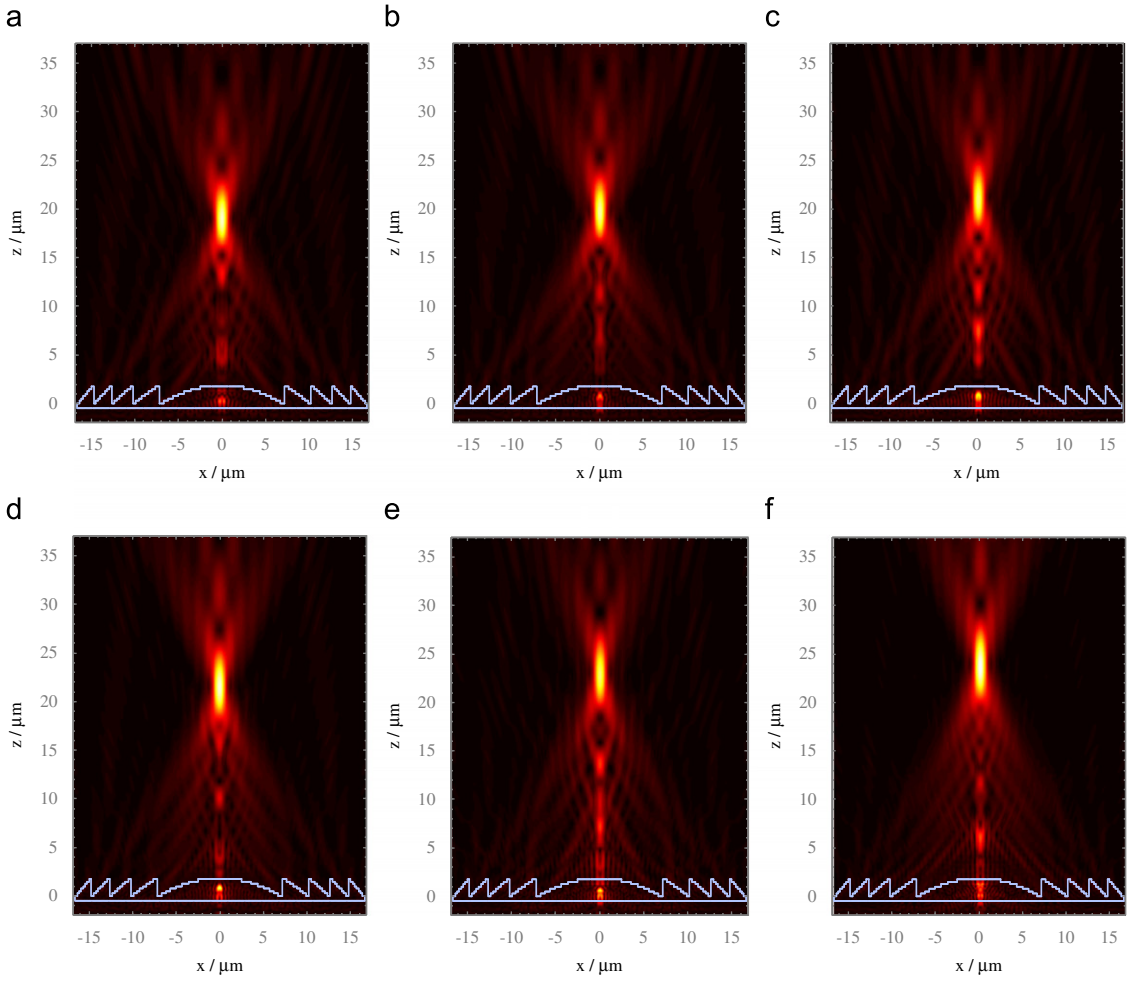

Fig. 3. Diffraction distribution of $|E|$ fields (a)–(f) when the DML is illuminated by normal incident monochromatic light with a wavelength of 1.30, 1.25, 1.20, 1.15, 1.10, and 1.05 μm, respectively.

FDTD simulation are shown in Fig. 5(a)–(d). There is a brighter focus with longer focal depth in the diffractive field and a higher order focus with shorter focal depth that gradually brightens when the illumination wavelength decreases.

Fig. 6 shows the normalised electric field amplitude along the optical axis for five incident wavelengths. The principal focal points correspond to the 1st-order focus. The principal focal lengths are 26.50, 28.30, 29.90, and 32.50 μm for illumination wavelengths of 0.95, 0.90, 0.85, and 0.80 μm, respectively. In Fig. 6, between 10 and 18 μm on the optical axis, it is apparent that the electric field amplitude of the 2nd-order focus increases as the illumination wavelength decreases. The focal depths for the 1st-order focuses are 4.2, 4.3, 4.4, and 4.7 μm for illumination wavelengths of 0.95, 0.90, 0.85, and 0.80 μm, respectively.

The illumination wavelengths for the second group are 0.75, 0.70, 0.65, 0.60, 0.55, 0.50, 0.45, 0.40, and 0.35 μm. The

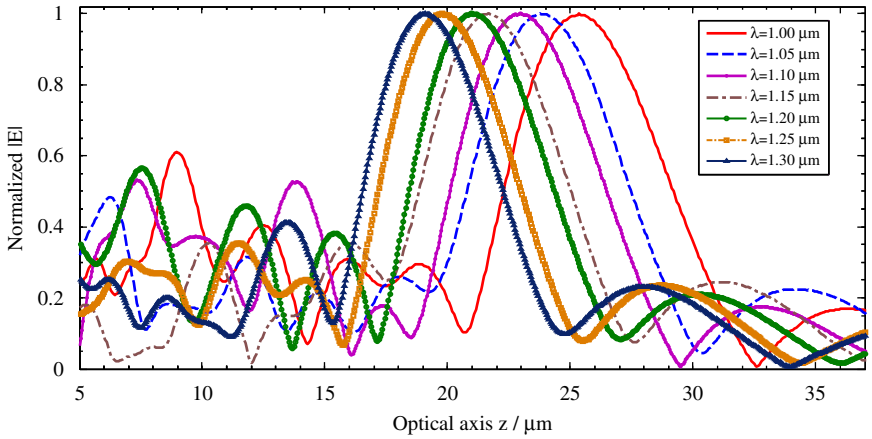

Fig. 4. Normalised $|E|$ along the optical axis for illumination wavelengths of 1.00, 1.05, 1.10, 1.15, 1.20, 1.25 and 1.30 μm.

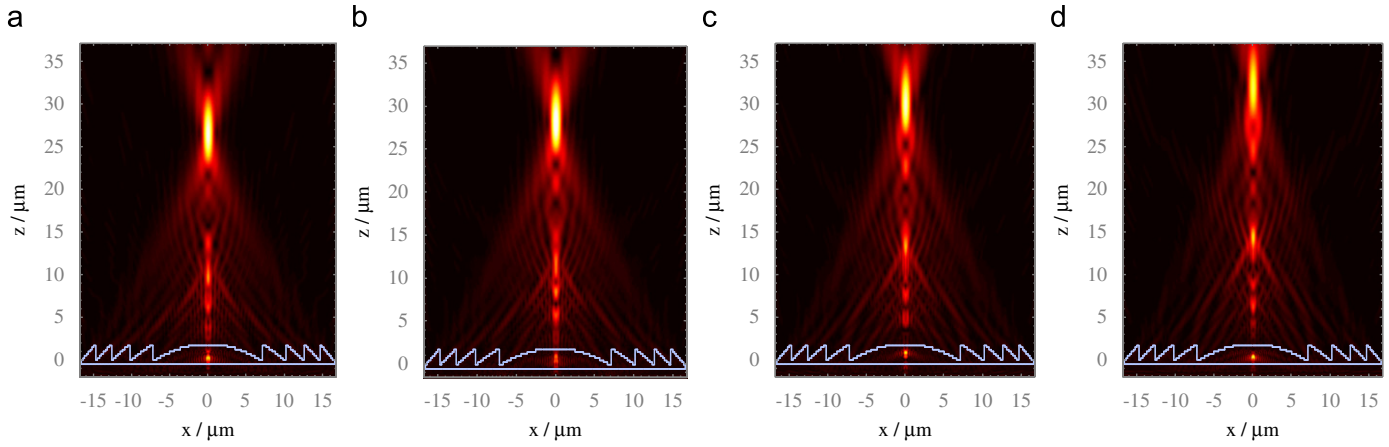

Fig. 5. Diffraction distribution of the $|E|$ fields (a)–(d) when the DML is illuminated by normal incident monochromatic light with wavelengths of 0.95, 0.90, 0.85, and 0.80 μm, respectively.

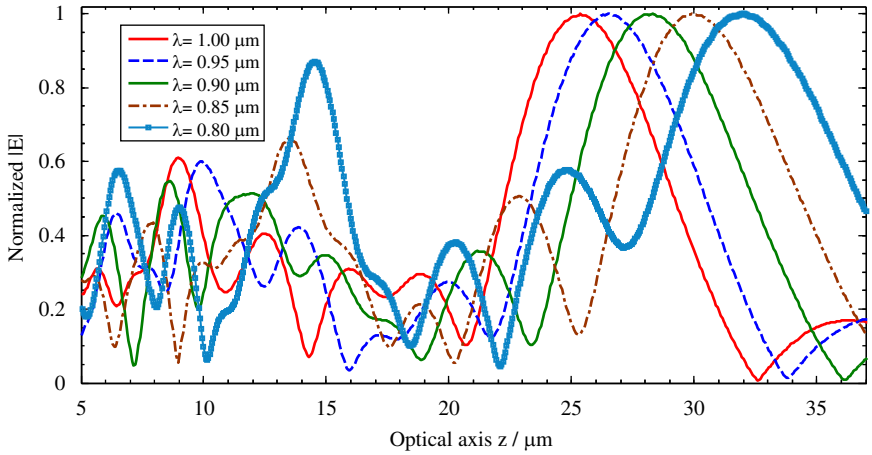

Fig. 6. Normalised $|E|$ along the optical axis for illumination wavelengths of 1.00, 0.95, 0.90, 0.85, and 0.80 μm.

corresponding simulation results are shown in Fig. 7(a)–(i). Because the 1st-order focal length increases when the illumination wavelength decreases, the simulation space was extended to illustrate all diffractive order foci. The space in the z-direction extends to a distance slightly longer than 50 μm. Fig. 8 (a)–(b) shows the normalised electric field amplitude along the optical axis for these illumination wavelengths.

In Fig. 7, several foci appeared in the diffractive field. The diffractive order of focus can be simply distinguished by the rule: the higher the diffractive order, the shorter the focal length. From Fig. 7(a)–(f), it is obvious that the brightness of 1st-order focus decreases and the brightness of 2nd-order focus increases with decreasing incident wavelength. In Fig. 8(a), between 30 and 45 μm on the optical axis, the electric field amplitude of 1st-order focus significantly decreases as the incident wavelength

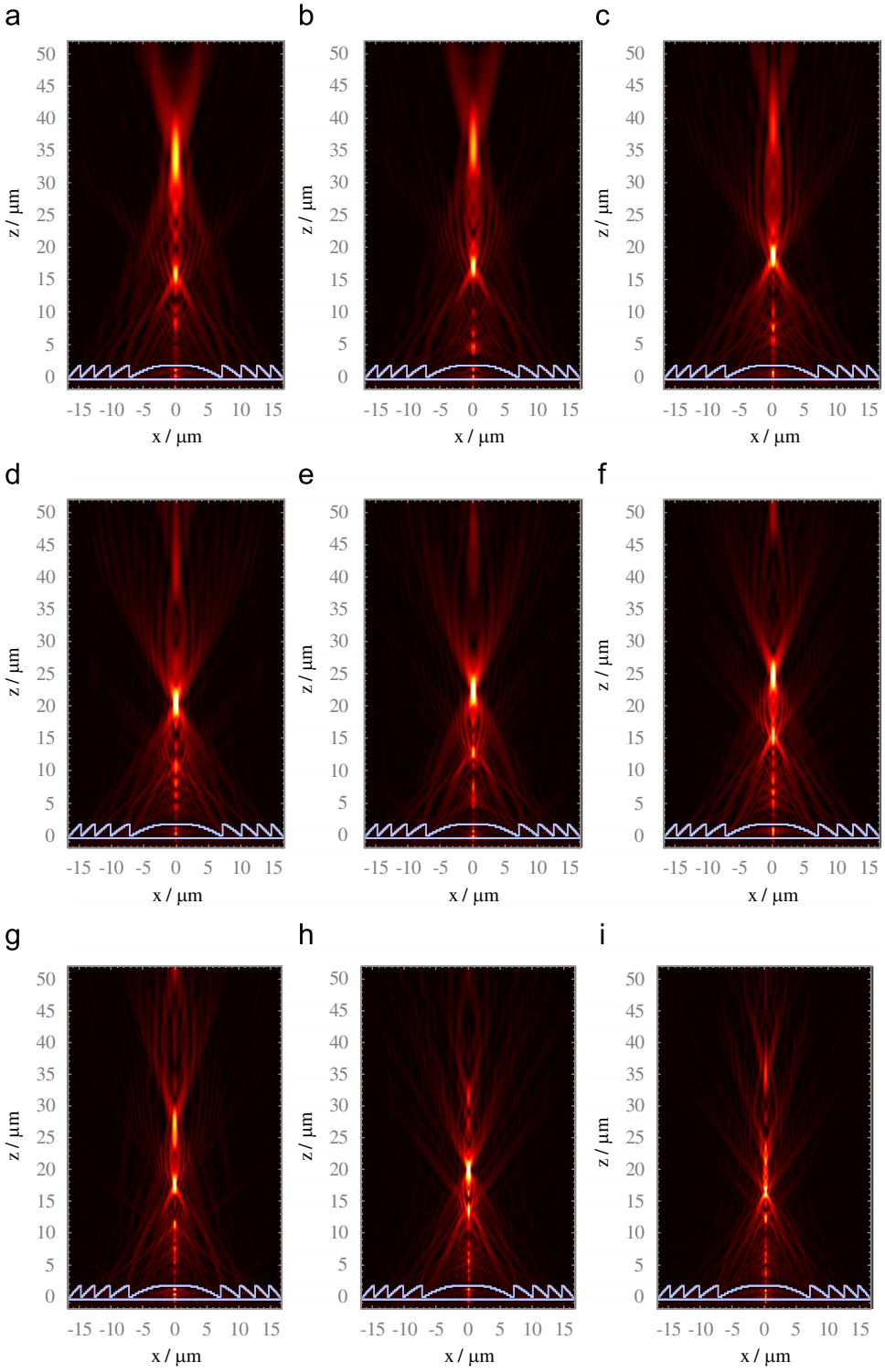

Fig. 7. Diffractive distribution of $|E|$ fields (a)–(i) when the DML is illuminated by normal incident monochromatic light with wavelengths of 0.75, 0.70, 0.65, 0.60, 0.55, 0.50, 0.45, 0.40, and 0.35 μm, respectively.

decreases. From Fig. 8(a), it is also found that the 2nd-order focus has the maximum electric field amplitude. For illumination wavelengths of 0.75, 0.70, 0.65, 0.65, and 0.55 μm, the principal foci correspond to the 2nd-order foci with principal focal lengths of 16.15, 17.05, 18.55, 20.45, and 22.45 μm, and focal depths of 1.6, 1.7, 1.8, 1.9, and 2.1 μm, respectively. From Fig. 7(e)–(h), a decrease in the brightness of 2nd-order focus with a concomitant increase in the brightness of the 3rd-order focus was observed. From Fig. 8(b), the electric field amplitude of the 2nd-order focus decreases with decreasing incident wavelength. In addition, there are two peaks for the illumination wavelength of 0.50 μm that correspond to the 2nd-order and the 3rd-order foci. The electric field amplitude of the 2nd-order focus is slightly higher than that for the 3rd-order focus. At an incident wavelength of 0.50 μm, the principal focus is still the 2nd-order focus, with a corresponding principal focal length of 24.50 μm and a focal depth of 2.3 μm. For

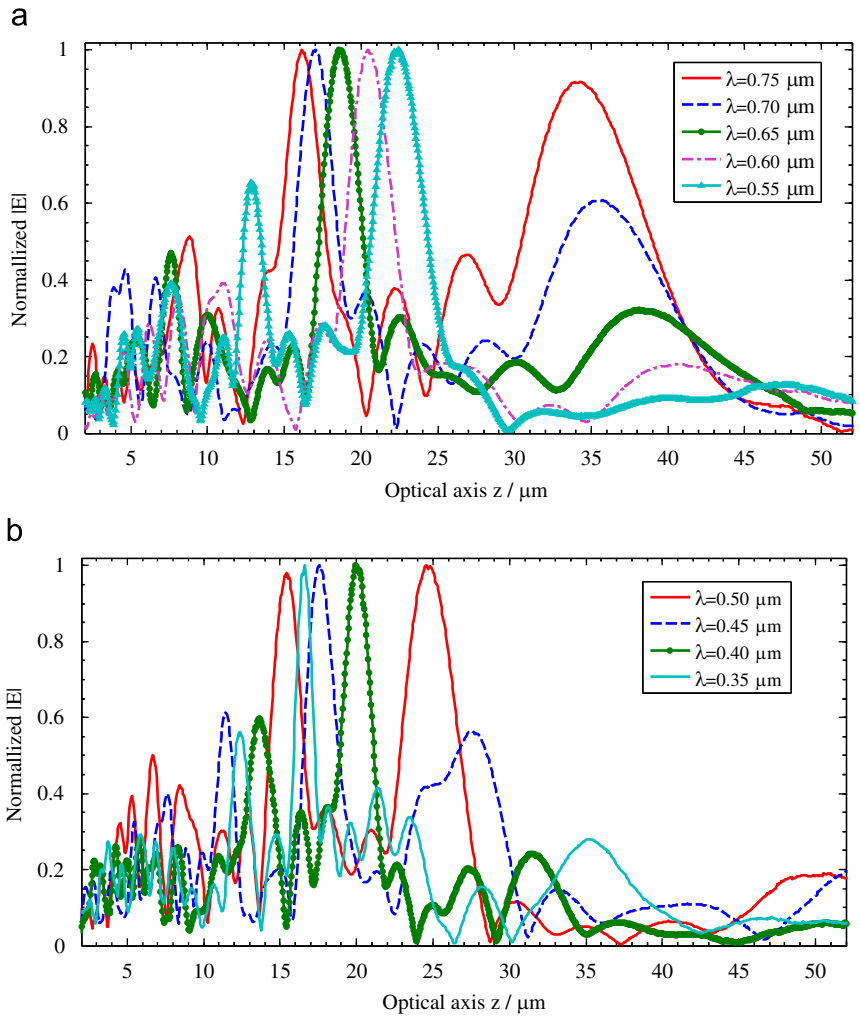

Fig. 8. Normalised $|E|$ along the optical axis for illumination wavelengths of 0.75, 0.70, 0.65, 0.60, 0.55 μm (a) and for illumination wavelengths of 0.50, 0.45, 0.40, and 0.35 μm (b).

wavelengths of 0.45 and 0.40 μm, however, the 3rd-order foci have the maximum electric field amplitudes with principal focal lengths of 17.55 and 19.95 μm and focal depth of 1.3 and 1.2 μm, respectively. Also, the principal focus is of the 4th-order for an illumination wavelength of 0.35 μm with a principal focal length of 16.60 μm and a focal depth of 0.80 μm.

4.4. Dispersion curve that shows broadband dispersion characteristics of the DML

Based on the above simulation results, dispersion curves for the analysed DML are plotted (Fig. 9). The dispersion curve for the DML illustrates the relationship between the principal focal length and the illumination wavelengths. It consists of four segments: in wavelengths between 0.80 and 1.30 μm, which is near the designed wavelength of 1 μm, the principal foci correspond to 1st-order foci; in wavelengths between 0.50 and 0.75 μm, the principal foci correspond to 2nd-order foci; in wavelengths between 0.40 and 0.45 μm, the principal foci correspond to 3rd-order foci; and finally for an illumination wavelength of 0.35 μm, the principal focus corresponds to 4th-order focus. The dispersion curve is not continuous because not only the principal focus changes to higher diffraction orders when the illumination wavelength decreases, but the higher diffraction order focus also has a shorter focal length (see Fig. 1).

Fig. 10 shows the focal depth and the principal focal length versus the illumination wavelength, where the vertical coordinate of the centre of the bar represents the principal focal length while the height of the bar represents the depth of focus. The four different segments representing different diffractive orders are denoted with bars of different colours in Fig. 10. Comparing the four segments, the lower diffractive order focus has a longer focal depth. However, the focal depth decreases with increasing wavelengths within the same diffractive order. Moreover, for broadband illumination light, DMLs can focus discrete wavebands to a common position. For example, a DML can focus light in the waveband near a wavelength of 0.50 μm and a waveband of 0.95–1.10 μm at a focal length of 25 μm. Such focusing can be found for some other wavebands in Fig. 10. The broadband dispersion characteristics of DML will benefit applications such as optical coupling for broadband fibre sources.

5. Discussions

In this paper, the broadband dispersion characteristics of DML are studied using the FDTD method. The simulation results clearly show that the higher focusing energy transfers from lower diffractive order to higher diffractive order when the illumination wavelength decreases within 0.35–1.30 μm. The dispersion curve of the analysed DML is presented. From the dispersion curve, the

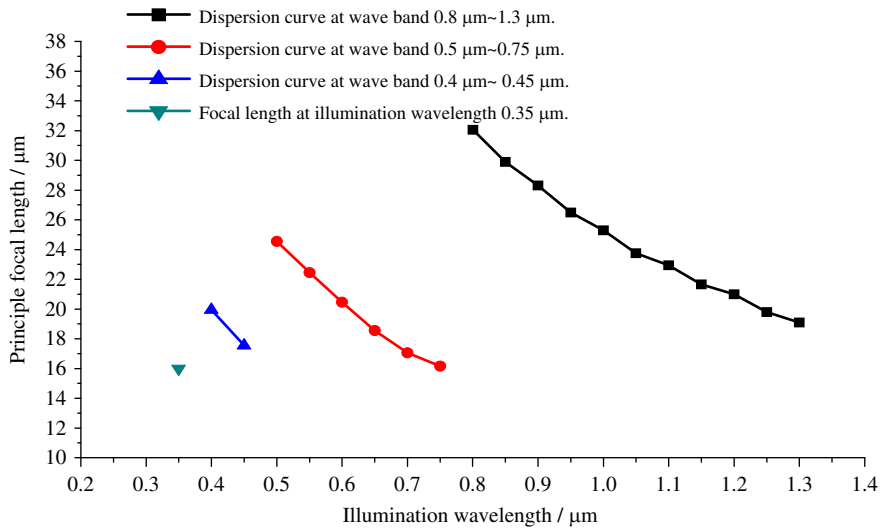

Fig. 9. Dispersion curve for the DML based on FDTD numerical results for illumination wavelengths between 0.35 and 1.30 μm.

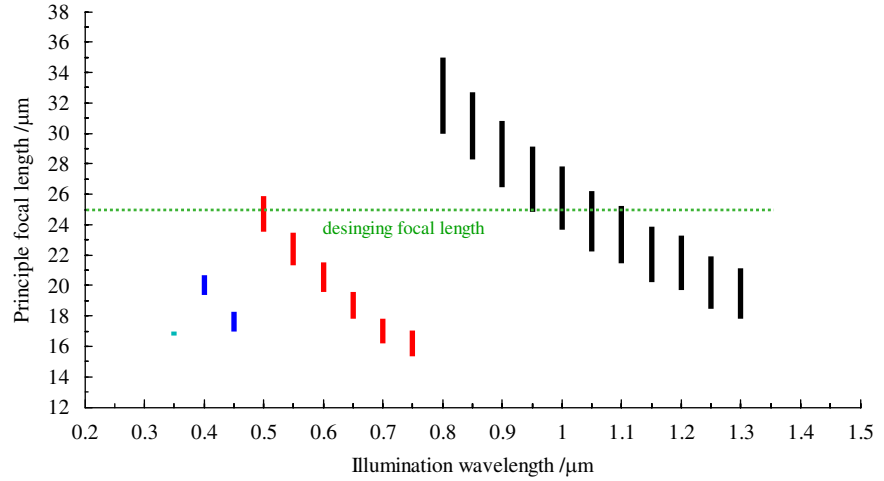

Fig. 10. Principal focal lengths of the DML for wavelengths between 0.35 and 1.30 μm, where the bar height represents the focal depth.

relationship between the principal focal lengths and the illumination wavelengths can be obtained. The broadband dispersion curve is discontinuous because the diffraction order of the principal focal point varies with illumination wavelength. Within a continuous segment of the dispersion curve, the principal focal length decreases with increasing illumination wavelengths. From the entire dispersion curve, however, different discrete wavebands may have overlapping focus positions.

The broadband dispersion characteristics of DML can be used to solve optical coupling problem, especially for broadband fibre sources. Depending on the design formula of DML in Section 2, the design wavelength and the focal length can be chosen at will. The results in this paper show that the waveband around the designed wavelength and waveband around half of the designed wavelength can be focused to the same spatial position. This observation can guide people to design a DML, for a given waveband, that focuses light within this waveband onto the same spatial location to optimise the coupling efficiency.

Because the dispersion of a diffractive lens is mainly induced by wavelength as opposed to the refractive index, a change in the wavelength-dependent refractive index is not considered in this paper. If DML users are interested in the effect of both the wavelength and refractive index on the dispersion, they can change the DML refractive index with the wavelength when they perform the FDTD simulation. In addition, as demonstrated in this paper, the dispersion curve is not continuous for a wide range of wavelengths, so a careful study of design principles for choosing the cut-off wavelength warrants further investigation.

Acknowledgments

This work was supported by the National Natural Scientific Foundation of China under Grants 60777034 and 10704072. We thank the reviewers very much for giving us insightful comments and constructive advice.

References

[1] Prasciolu M, Cojoc D, Cabrini S, Businaro L, Candeloro P, et al. Design and fabrication of on-fiber diffractive elements for fiber-waveguide coupling by means of e-beam lithography. Microelectron Eng 2003;67–68:169–74.
[2] Nishizawa Norihiko, Mitsuzawa Hideyuki, Takayanagi Jun, Sumimura Kazuhiko. Generation of 0.45–1.38 μm visible to near-infrared widely broadened supercontinuum using Er-doped ultrashort-pulse fiber laser system. J Opt Soc Am B 2009;26:426–31.
[3] Roy Sourabh, Roy Chaudhuri Partha. Supercontinuum generation in visible to mid-infrared region in square-latticephotonic crystal fiber made from highly nonlinear glasses. Opt Commun 2009;282:3448–455.

[4] Shi Kebin, Li Peng, Liu Zhiwen. Broadband coherent anti-Stokes Raman scattering spectroscopy in supercontinuum optical trap. Appl Phys Lett 2007;90(141116):1–3.
[5] Hartl XD, Li C, Chudoba RK, Ghanta TH, Ko JG, Fujimoto JK, Ranka, Windeler RS. Ultrahigh-resolution optical coherence tomography using continuum generation in an air–silica microstructure optical fiber. Opt Lett 2001;26:608–10.
[6] Morioka T, Kawanishi S, Mori KSaruwatari. Transform-limited, femtosecond WDM pulse generation by spectral filtering of gigahertz supercontinuum. Electron Lett 1994;30:1166–8.
[7] Faklis Dean, Michael Morris G. Spectral properties of multiorder diffractive lenses. Appl Opt 1995:2462–8.
[8] Sweeney Donald W, Gary ESommargren. Harmonic diffractive lens. Appl Opt 1995:2469–75.
[9] Taflove Allen, Hagnness Suan C. Computational Electrodynamics: The Finite-Difference Time-Domain Method. Boston, Mass: Artech House; 2000.
[10] Yuling Liu, Hua Liu. Rigorous vector analysis of diffractive microlens by using of finite-difference time-domain method. In: Proceeding of SPIE 2009; vol. 7506.